



HAL
open science

An easy to implement and robust design control method dedicated to multi-cell converters using inter cell transformers

Khaled Tamizi, Olivier Béthoux, Eric Labouré

► To cite this version:

Khaled Tamizi, Olivier Béthoux, Eric Labouré. An easy to implement and robust design control method dedicated to multi-cell converters using inter cell transformers. *Mathematics and Computers in Simulation*, 2020, 167, pp.461 - 477. 10.1016/j.matcom.2019.02.004 . hal-02118667

HAL Id: hal-02118667

<https://hal.science/hal-02118667v1>

Submitted on 3 May 2019

HAL is a multi-disciplinary open access archive for the deposit and dissemination of scientific research documents, whether they are published or not. The documents may come from teaching and research institutions in France or abroad, or from public or private research centers.

L'archive ouverte pluridisciplinaire **HAL**, est destinée au dépôt et à la diffusion de documents scientifiques de niveau recherche, publiés ou non, émanant des établissements d'enseignement et de recherche français ou étrangers, des laboratoires publics ou privés.



Accepted Manuscript

An Easy to Implement and Robust Design Control Method Dedicated To Multi-Cell Converters Using Inter Cell Transformers

Khaled Tamizi, Olivier Béthoux, Eric Labouré

DOI: [10.1016/j.matcom.2019.02.004](https://doi.org/10.1016/j.matcom.2019.02.004)

Reference:

Publisher: ELSEVIER

To appear in: ***Mathematics and Computers in Simulation***

Received date: 15 January 2018

Revised date: 2 October 2018

Accepted date: 1 February 2019

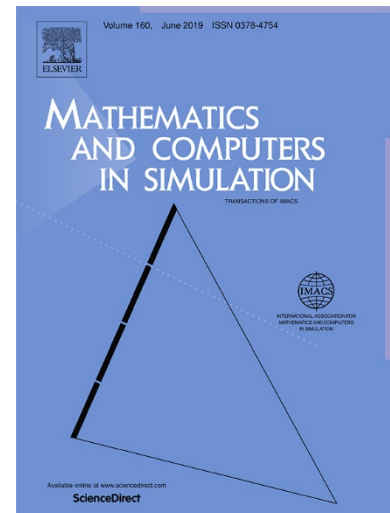
Date of Publication: 12 March 2019 (online)

To be published in (Volume XXX, Pages YY-ZZ)

Please cite this article as: K. Tamizi, O. Béthoux, E. Labouré, An easy to implement and robust design control method dedicated to multi-cell converters using inter cell transformers, *Mathematics and Computers in Simulation*, 2019, ISSN 0378-4754, <https://doi.org/10.1016/j.matcom.2019.02.004>.

Document Version: Early version, also known as pre-print

This is a PDF file of an unedited manuscript that has been accepted for publication. As a service to our customers we are providing this early version of the manuscript. The manuscript will undergo copyediting, typesetting, and review of the resulting proof before it is published in its final form. Please note that during the production process errors may be discovered which could affect the content, and all legal disclaimers that apply to the journal pertain.



1 An Easy to Implement and Robust Design

2 Control Method Dedicated To Multi-Cell

3 Converters

4 Using Inter Cell Transformers

5 K. Tamizi, O. Béthoux*, E. Labouré

6 GeePs | Group of Electrical Engineering – Paris

7 UMR CNRS 8507, CentraleSupélec, Univ Paris-Sud, Sorbonne Universités, UPMC Univ Paris

8 06

9 Gif-sur-Yvette, France-

10 * olivier.bethoux@centralesupelec.fr

11
12 **CORRESPONDING AUTHOR:** Olivier BETHOUX, Full Professor, UPMC Univ Paris, France

13 **AFFILIATION:** GEEPS | GROUP OF ELECTRICAL ENGINEERING – PARIS

14 **EMAIL:** olivier.bethoux@centralesupelec.fr

15 **TEL:** +33(0)169851656

16 **FAX:** + 33(0)169418318

17

1 **ABSTRACT**

2 Parallel multi-cell converters using inter-cell transformers are real multi-input multi-output
3 systems, making their control challenging and possibly requiring increased embedded computing
4 power in the control architecture. The challenge of the current study is to design a control algorithm
5 as simple as possible, in terms of settings and implementation, while meeting standard
6 specification. The state-space representation of multi-cell converters permits to define a full state
7 feedback. Such Multi-Input Multi-Output (MIMO) systems have numerous tuning parameters
8 which enable various ways to tackle the control specifications. Among the specific approaches,
9 both total decoupling and optimal control based on quadratic cost and objective functions are
10 addressed thoroughly and consistently. The studied case is a 3-cell parallel converter for which
11 various settings of the state feedback are considered and analyzed by simulation. Linear-quadratic
12 regulator design reveals the best compromise between variables tracking precision and robustness
13 towards system parameters and load variation. Furthermore it is easy to implement utilizing few
14 non-zero setting coefficients. Specifically the feedback gain matrix associated to the integral terms
15 is almost diagonal: this natural decoupling makes it extremely simple to efficiently implement an
16 anti-windup algorithm. This is an important result since until now, the standard solution is mostly
17 based on decoupling strategies. Among other drawbacks, this latter approach proves to be much
18 more sensitive to parameter uncertainties.

19 **KEYWORDS**

20 Photovoltaic power converter, Multicell converter, InterCell Transformer (ICT) [1], multi input
21 multi output system (MIMO), robust control, sensitivity analysis, Linear quadratic regulator
22 (LQR), antiwindup.

1 **1. INTRODUCTION**

2 Parallel multi-cell converters using inter cell transformers (ICTs) are an attractive technique in the
3 field of low and medium voltage and high current power converters. These very versatile structures
4 can be used in many types of power conversion structures such as Boost or Buck DC-to-DC power
5 converters as well as in DC-to-AC inverters or AC-to-DC synchronized rectifiers. They are broadly
6 used in various applications and are particularly useful in renewable energy systems such as in
7 photovoltaic inverters [2, 3], storage management systems [4], fuel cell converters [5] as well as in
8 electrical vehicle [6]. Notwithstanding this success, there is scope for further improvements, such
9 as ICT design for fault-operation [7] and control enhancement [8, 9]. The present article focuses
10 on this latter point from a control engineering practice point of view.

11 On a very broad basis, fractioning power shows many advantages. When interleaved generated
12 Pulse Width Modulation (PWM) patterns are used, it enables to significantly reduce the switching
13 stress due to interconnections leakage energy leading to voltage overshoot and electromagnetic
14 interferences and the harmonic spectrum. This also allows a significant decrease of input and output
15 filters size. The best performances are obtained in multi-cell converters when the converter is
16 designed with one or several magnetic ICTs instead of individual inductors [1]. With respect to this
17 final point, the ICT has to figure an important coupling effect to achieve good performances
18 (compactness, power efficiency, current constraints). From a control point of view this magnetic
19 coupling makes the power stage switch from several single input single output (SISO) systems to
20 a unique multi input multi output (MIMO) system. Despite this change, the challenge is to keep
21 the dedicated control algorithm as simple as possible, in terms of settings and implementation. It
22 aims at providing an efficient control, both robust regarding system uncertainties and easy to
23 implement in a classic microcontroller.

1 The literature shows that the study of the ICT multicell converter control has already been
2 undertaken. First, Bolloch et al. have elaborated a strategy permitting a relevant steady state
3 behavior without deeply studying the dynamic behavior of the control scheme [8]. Then, Gautier
4 et al. have proposed a strategy based on decoupling matrices which permits to control the natural
5 modes of the converter with independent PI controllers [9]. This unique solution based on a
6 practical approach leads to a single solution which has not really been considered in a broader
7 context permitting to assess its performances regarding other solutions. On a more specific issue,
8 sensitivity analysis regarding parameters uncertainties are not assessed. Amghar et al. have
9 explored another possible control technique based on a combination of PI controller and Petri nets
10 method [10]. It requires very high sampling rates to operate properly and, in the submitted work,
11 the magnetic coupling effect has not yet been taken into account. Based on Finite-state machine,
12 Petri nets number of states increase exponentially with the number of cells, making it demanding
13 on computational resources.

14 Among the previous studies, classical PI controllers can be achieved with relatively small
15 computational resources. The accurate adjustment of their settings, the impact of system parameters
16 uncertainties, the functioning under saturation have not been yet addressed. The present
17 investigation is carrying out a comprehensive study of state-feedback controller. It considers the
18 different ways to tune its control settings with respect to system parameter sensitivity, decoupling
19 behavior and the ease of implementation including control during saturation. For this purpose, the
20 ICT converter is studied in the general framework of state representation. The present work exhibits
21 the available degrees of freedom and argues on their best use. The control performance criteria are
22 assessed regarding parameter uncertainties in order to address robustness key issue. Specific focus

1 is also given to implementation issues. In addition, the theoretical study is supplemented with
2 simulation results based on a 3-cell ICT converter.

3 The manuscript is organized as follows. After this short introduction, section II presents the
4 control model of a 3-cell interleaved multi-cell DC-DC buck converter and details the
5 specifications related to the PV application under study. The third section presents the state
6 feedback controller and considers the various possibility of tuning its numerous parameters. The
7 fourth section addresses the particular tuning choice which permits to cancel coupling effects
8 between the cells. The fifth section considers another design method based on the optimization of
9 a quadratic optimization function, named LQR approach [11]. The sixth part undertakes a
10 comprehensive comparative study of both considered approaches; for this purposes numerous
11 scenarios are simulated and analyzed. Finally, the paper ends with conclusions and future
12 prospects.

13

14 **2. MULTI-CELL INTERLEAVED BUCK CONVERTER AND ITS CONTROL-ORIENTED MODEL**

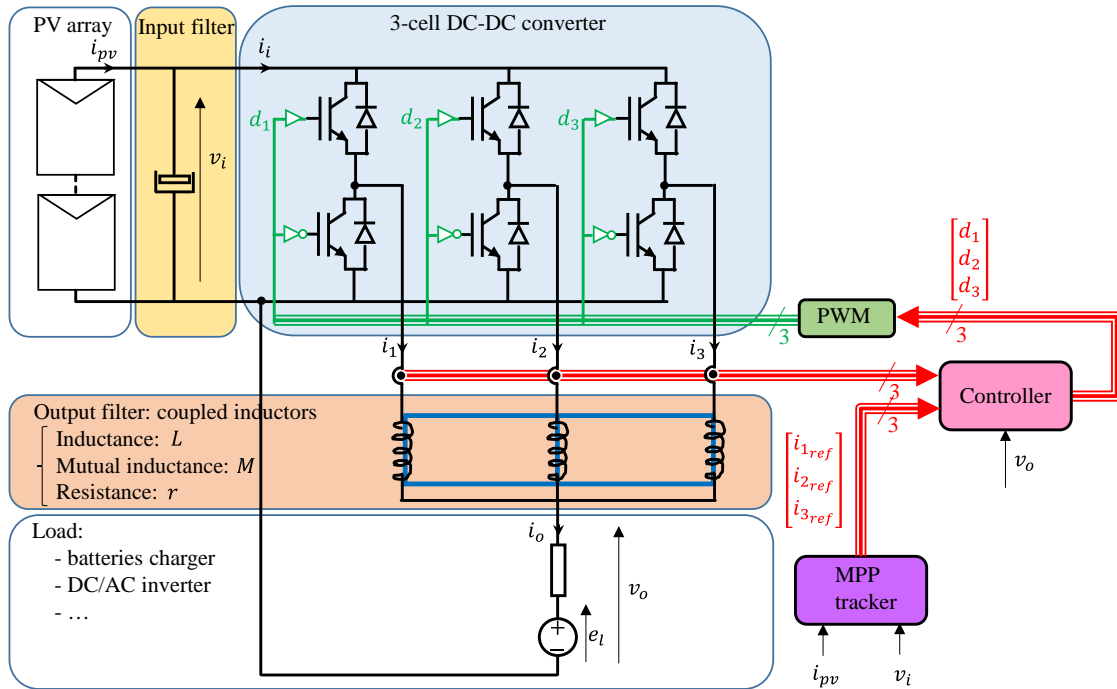
15 2.1. Multi-cell interleaved buck converter for solar application.

16 Figure 1 depicts the system under study. A photovoltaic array feeds a load which could be possibly
17 a battery directly powering DC loads or a grid inverter [12]. As both PV maximum power point
18 and the load voltage can vary greatly, it is mandatory to interface a converter between the load and
19 the source: this is the multi-cell converter using a monolithic ICT formed by n windings wounded
20 on the same magnetic circuit. For simplicity, it has three switching cells ($n = 3$) and a 3-phase-
21 transformer acting as an output current filter. The input current is filtered by the input capacitor C_i .
22 Each switching cell is driven by a PWM control signal characterized by a constant switching
23 frequency f and a duty cycle d_k , which represents a system control variable. The system

1 parameters and the rated variables are listed in Table 1.

2 Compared to classic single buck converter, the main advantage of this power electronics structure
3 is to ensure low current ripples at both input and output sides. In fact, regarding the input stage, the
4 input current ripple is reduced by an n factor while the input current apparent frequency is increased
5 by a factor of n . As a result, the C_i capacitance can be reduced by a significant n^2 factor leading to
6 improve the system dynamics and namely its ability to track faster the maximum power point of
7 the PV array. Similarly, the amplitude of phase current ripples are reduced by a n^2 factor compared
8 to an uncoupled multi-cell converter (considering a similar filtering inductance value), which
9 reduces the constraints on the power semi-conductors and the related losses. Moreover, the global
10 power converter output current ripple is reduced by n compared to a classical one-cell Buck DC-
11 DC converter, in the same way as for interleaved multi-cell DC-DC Buck converter with uncoupled
12 inductors. This limits the need to filter the output voltage: in some cases, no additional output
13 capacitor is required.

14 These electrical and energetics advantages are counterbalanced by a rising difficulty to control
15 the system in static and dynamic conditions. This is why a control-orientated model is needed to
16 study the feedback control.



1
2

Fig. 1. Multi-cell coupled power architecture.

| Symbol | Quantity | Value |
|----------------|--------------------------------|------------------|
| v_i | PV panel array voltage | 400 (V) |
| $I_{i, rated}$ | PV panel array current | 9.25 (A) |
| f | Cell switching frequency | 20 (kHz) |
| C_i | Input capacitance | 2 (mF) |
| l | ICT self-inductance | 20.0 (mH) |
| m | ICT mutual inductance | 9.5 (mH) |
| r | ICT rated phase resistance | 0.2 (Ω) |
| r_l | Rated load resistance | 0 (Ω) |
| $i_{l, max}$ | Short circuit current protect. | 15 (A) |
| e_l | Rated load voltage source | 200 (V) |
| l_{min} | Minimum ICT self-induct. | 19.7 (mH) |
| m_{max} | Maximum ICT mutual induct. | 9.7 (mH) |
| r_{max} | Maximum ICT phase resist. | 0.5 (Ω) |

3
4

Tab. 1. System parameters.

5 2.2. Control-oriented models of multi-cell interleaved buck converter.
 6 For general purpose, the power converter model uses the following assumptions:
 7 - Regarding the closed loop response time of the controlled system, PV array behaves as a

1 perfect voltage source. The input voltage of the power converter v_i is therefore imposed in
 2 the model.

3 - The load fed by the power converter can represent different types of loads and is assumed to
 4 be linear. It is considered as a Thévenin's equivalent circuit consisting of an equivalent
 5 voltage source e_l in series connection with an equivalent impedance Z_l . The following
 6 developments only consider the pure real case, namely: $Z_l = r_l$. Finally, the DC load is hence
 7 described by:

$$8 \quad v_o = e_l + r_l i_o \quad (1)$$

9 where v_o and i_o are the output voltage and current, respectively.

10 - The monolithic ICT is also considered as linear and is represented by three magnetically
 11 coupled electrical equations. For a 3-leg symmetrical monolithic ICT the mutual inductances
 12 are identical with a negative value and are denoted $(-m)$ in the following model while l is
 13 the winding self-inductance:

$$\begin{bmatrix} v_{L1} \\ v_{L2} \\ v_{L3} \end{bmatrix} = \begin{bmatrix} l & -m & -m \\ -m & l & -m \\ -m & -m & l \end{bmatrix} \frac{d}{dt} \begin{bmatrix} i_1 \\ i_2 \\ i_3 \end{bmatrix} + \begin{bmatrix} r & 0 & 0 \\ 0 & r & 0 \\ 0 & 0 & r \end{bmatrix} \begin{bmatrix} i_1 \\ i_2 \\ i_3 \end{bmatrix} \quad (2)$$

14 - The 3 switching cells are controlled by 3 binary control variables u_k , operating at a constant
 15 switching frequency T_S . For the purpose of designing a control scheme, only the average cell
 16 behavior is considered; the system control inputs are the 3 duty-cycles of each cell $d_k =$
 17 $\langle u_k \rangle_{T_S}$ which have a limited range from 0 to 1. Duty cycles saturation should therefore be
 18 managed by the controller. This technical point has to be taken into account properly to obtain
 19 an efficient real-time implementation.

20 With these assumptions, the Kirchhoff's current law gives the link between output current

1 and ICT's inner currents:

2

$$i_o = i_1 + i_2 + i_3 \quad (3)$$

3

4 while the 3 Kirchhoff's voltage laws of the global system show the link between control

5 values d_k , output voltage v_o and inner ICT's voltages v_{Lk} :

6

$$v_i \begin{bmatrix} d_1 \\ d_2 \\ d_3 \end{bmatrix} = \begin{bmatrix} v_{L1} \\ v_{L2} \\ v_{L3} \end{bmatrix} + \begin{bmatrix} v_o \\ v_o \\ v_o \end{bmatrix} \quad (4)$$

7

8 Using previous equations, namely (1) to (4) enables to obtain the converter average model.

9 It is written in the state-space representation as follows:

$$\frac{d}{dt} \begin{bmatrix} i_1 \\ i_2 \\ i_3 \end{bmatrix} = -\frac{1}{(l-2m)(l+m)} \begin{bmatrix} l-m & m & m \\ m & l-m & m \\ m & m & l-m \end{bmatrix} \begin{bmatrix} r+r_l & 0 & 0 \\ 0 & r+r_l & 0 \\ 0 & 0 & r+r_l \end{bmatrix} \begin{bmatrix} i_1 \\ i_2 \\ i_3 \end{bmatrix} \quad (5)$$

$$+ \frac{v_i}{(l-2m)(l+m)} \begin{bmatrix} l-m & m & m \\ m & l-m & m \\ m & m & l-m \end{bmatrix} \begin{bmatrix} d_1 \\ d_2 \\ d_3 \end{bmatrix} - \frac{1}{(l-2m)} \begin{bmatrix} 1 \\ 1 \\ 1 \end{bmatrix} e_l$$

10 With $\mathbf{I} = [i_1 \ i_2 \ i_3]^t$ the state vector whose 3 components are the 3 ICT inner currents,

11 $\mathbf{D} = [d_1 \ d_2 \ d_3]^t$ the control vector and e_l the scalar perturb input.

12 It is worth noting that the load voltage source represents a battery or the capacitive input filter

13 of an inverter. This mean that the series resistance r_l is low and can be neglected in a first

14 approach. With this assumption, the resulting state-space representation is:

15

$$\frac{d}{dt}\mathbf{I} = \mathbf{A}\mathbf{I} + \mathbf{B}\mathbf{D} + B_p e_t \quad (6)$$

1 With A the state matrix and B the control matrix and B_p the perturb matrix described as:

$$2 \quad A = \frac{-r}{(l-2m)(l+m)} \begin{bmatrix} l-m & m & m \\ m & l-m & m \\ m & m & l-m \end{bmatrix}$$

$$3 \quad B = \frac{v_i}{(l-2m)(l+m)} \begin{bmatrix} l-m & m & m \\ m & l-m & m \\ m & m & l-m \end{bmatrix}$$

$$4 \quad B_p = -\frac{1}{(l-2m)} \begin{bmatrix} 1 \\ 1 \\ 1 \end{bmatrix}$$

5 Note that the term r is voluntary not factored into the state equation to underline that the
 6 forthcoming robustness analysis of each control strategy considers individual winding
 7 resistance variation.

8 Functionally, the output current i_o , sum of the three winding currents (3), is the only variable
 9 which should be controlled. In actual experience, the converter faces discrepancies at several level
 10 (winding and switch resistances due to temperature difference, actual duty cycle of the switch due
 11 to non-identical dead-time, as examples) which may generate large DC current mismatch between
 12 each winding. It is hence mandatory to control each individual current i_k . In this context, the output
 13 vector is the state vector.

14 2.3. Model analysis.

15 From an engineer point of view, it is important to describe the model behavior regarding the
 16 single common mode and the two differential modes, named com and $diff_1$, $diff_2$, respectively
 17 and defined by the following relations:

18

$$\begin{cases} x_{com} = (1/3) \cdot (x_1 + x_2 + x_3) \\ x_{diff1} = x_1 - x_2 \\ x_{diff2} = x_2 - x_3 \end{cases} \quad (7)$$

1
 2 Indeed, in normal operating mode, the supervisor splits the output current demand into three
 3 similar ICT's inner current. Hence, only the common mode is solicited while the two other
 4 differential modes remain zero. Conversely, while a default occurs like a local overheat affecting
 5 a specific cell, the supervisor decreases the related current and increases the two other ones creating
 6 no common change but two differential mode changes.

7 Substituting (7) in the state equation derives the open loop modes' behavior:

$$\begin{cases} \frac{d}{dt} i_{com} = -\frac{1}{\tau_{com}} i_{com} + \frac{v_i}{(l-2m)} d_{com} - \frac{1}{(l-2m)} e_l \\ \frac{d}{dt} i_{diff1} = -\frac{1}{\tau_{diff}} i_{diff1} + \frac{v_i}{(l+m)} d_{diff1} \\ \frac{d}{dt} i_{diff2} = -\frac{1}{\tau_{diff}} i_{diff2} + \frac{v_i}{(l+m)} d_{diff2} \end{cases} \quad (8)$$

9 with τ_{com} and τ_{diff} the two different time constants of common mode and differential mode,
 10 respectively:

$$\tau_{com} = \frac{(l-2m)}{r}$$

$$\tau_{diff} = \frac{(l+m)}{r}$$

13 For the converter under study, the evaluation of the time constant values ratio is:

14

$$\frac{\tau_{com}}{\tau_{diff}} = \frac{l - 2m}{l + m} = \frac{1}{29.5} \quad (9)$$

1
2 It is hence clear that the open-loop system has two very different dynamics, which requires a
3 specific control design. By nature, the circulating current can change slowly, while the output
4 current can be adjusted very quickly, which is one of the main ICT's asset.

5 2.4. State feedback specifications.

6 The control design has to take this detailed analysis into account with relevant required dynamics.
7 The present study considers the specifications summarized in table 2. Indeed, the first requirement
8 is to guarantee a good precision in steady state in order to fulfill the maximum point tracker
9 requirements; the purpose of the present study is to cancel the steady state error. Second, the time
10 taken for the response to reach the desired set point is also important for the system functionality.
11 The solar converter needs to react to solar irradiance changes which in the worst case may occur
12 in a 10 ms time period, which is not very challenging. However, there are obviously other
13 scenarios to consider; short circuit limitation is one of the cases requiring a rapid action. For this
14 demanding challenge the settling time is set to 500 μs which means ten switching periods
15 ($T_s = 50 \mu s$). A third key point is to ensure a good stability margin of the closed loop system.
16 This point is achieved by satisfying an overshoot criteria and decay ratio. The overshoot criteria
17 gives also a good indication on how duty cycles saturations are managed and is set to a maximum
18 of 10%, while the decay ratio criteria gives a good performance index of the system stability and
19 is limited to a maximum 20% value. In addition, the minimization of the windings currents
20 coupling permits to control independently each phase current which is essential to modify the phase
21 power distribution in case of a local overheating; the limited overshoot while another current is

1 changing is a way to take this fact into account.

2 Finally, it is worth noting that the load voltage source represents a battery or the capacitive input
 3 filter of an inverter. Consequently, this voltage varies slowly and is measured for regulation
 4 purpose. Hence e_l represents a perturbation which can be simply cancelled by an additional
 5 feedforward term. More specifically, the control value D is the sum of two terms, one D_{e_l} computed
 6 using the output voltage measurement and the other one D' computed by the feedback law:

$$D = D_{e_l} + D' = \begin{bmatrix} e_l/v_i \\ e_l/v_i \\ e_l/v_i \end{bmatrix} + D' \quad (10)$$

8
 9 In sum, that is the reason why the load voltage source will no longer be considered, as mentioned
 10 in Table 1.

| Symbol | Quantity | Value |
|----------------------|--|----------------|
| ε_i | Steady state offset | 0 |
| τ_{i_o} | Time-response (settling time) | 500 (μ s) |
| $\Delta\%_{i_k/i_k}$ | Percentage overshoot regarding i_k subject to $i_{k,ref}$ setpoint change | 10% |
| $\Delta\%_{i_j/i_k}$ | Percentage overshoot regarding $i_{j \neq k}$ subject to $i_{k,ref}$ setpoint change | 10% |
| DR | Maximum decay ratio | 20% |

12
 13 **Tab. 2. Closed loop system specification.**

14

15 3. STATE FEEDBACK

16 The previous section described the power converter behavior using a state representation [13, 14].

17 It allowed to better understand the effects of the ICT magnetic coupling on the system. As it is easy

1 to monitor each state variable using 3 current sensors, full state feedback seems to be a very
2 appropriate control technique to adjust the characteristics of the closed loop system. A first step
3 gives the overall control structure. Then the state feedback setting is considered showing a great
4 number of possible tuning strategies. Among them, two specific methods showing particular
5 promise are identified.

6 3.1. Control structure and the related extended model.

7 The basic principle of state feedback [15, 16] is to place the closed loop system poles using the
8 following linear control law:

$$D = -KI + FI_{ref} \quad (11)$$

9 Where

- 10 - the $n \times n$ feedback matrix K enables to achieve the desired pole placement, which determines
11 the system behavior.
- 12 - the $n \times n$ pre-filter matrix $F = B^{-1}(BK - A)$ ensures a unit static gain between the
13 reference values and the measured values. It is important to stress that this matrix is calculated
14 with the state and control matrices (A and B) and thus strongly depends on the system
15 parameters.

16 Obviously, due to the mandatory pre-filter matrix, this first control structure is strongly dependent
17 on system parameters uncertainties. The way to deal with this is to add integral terms to the
18 feedback structure. It provides a suitable solution enabling to strengthen the overall feedback
19 robustness and guarantee no static error in any case. The idea is first to integer the errors between
20 the references and the related currents and then consider the three integer outputs as three additional
21 system states. Consequently the extended state dimension is $n_e = 2n = 6$ and its state
22 representation is described by:

$$\frac{d}{dt} \begin{bmatrix} \mathbf{I} \\ \mathbf{Int}_\varepsilon \end{bmatrix} = \begin{bmatrix} \mathbf{A} & \mathbf{0}_3 \\ -\mathbf{Id}_3 & \mathbf{0}_3 \end{bmatrix} \begin{bmatrix} \mathbf{I} \\ \mathbf{Int}_\varepsilon \end{bmatrix} + \begin{bmatrix} \mathbf{B} \\ \mathbf{0}_3 \end{bmatrix} \mathbf{D} + \begin{bmatrix} \mathbf{0}_3 \\ \mathbf{Id}_3 \end{bmatrix} [\mathbf{I}_{ref}] \quad (12)$$

1 3.2. Control structure degrees of freedom.

2 Similarly to the basic state feedback, the control values \mathbf{D} are calculated using the full state
 3 knowledge as depicted in figure 2. Note that the reference values \mathbf{I}_{ref} no longer act directly on the
 4 control values but through an integral path which filters the set point variations. Consequently, it
 5 avoids temporal overshoots of output values during fast transient.

6 To compute the 3 control values (i.e. \mathbf{D}), the state feedback linearly combines 6 states (i.e.
 7 $[\mathbf{I} \ \mathbf{Int}_\varepsilon]^t$). The following equation gives the related full feedback control law:

$$\mathbf{D} = -\mathbf{K}_e \begin{bmatrix} \mathbf{I} \\ \mathbf{Int}_\varepsilon \end{bmatrix} \quad (13)$$

8 The $n \times n_e$ feedback matrix $\mathbf{K}_e = [\mathbf{K}_{e1} \ \mathbf{K}_{e2}]$ has $n \times n_e = 18$ independent real parameters.
 9 For greater readability, the \mathbf{K}_e matrix is split into two submatrices. \mathbf{K}_{e1} represents a $n \times n$ matrix
 10 made of the n first \mathbf{K}_e columns: it contains the \mathbf{I} weighting parameters. Likewise, \mathbf{K}_{e2} is a similar
 11 matrix consisting of the n last \mathbf{K}_e columns and has the \mathbf{Int}_ε weighting parameters.

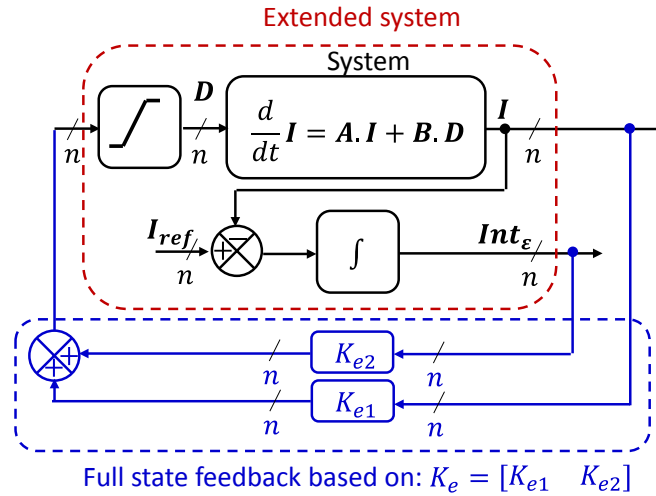
12 Adjusting the \mathbf{K}_e eighteen parameters permits to choose the $n_e = 6$ poles of the closed loop
 13 system which has a strong influence on the system's dynamics. It is thus evident that the \mathbf{K}_e matrix
 14 meeting this pole criteria is not unique. To take advantage of the opportunities offered by these too
 15 many coefficients, it is important to make explicit additional criteria permitting to strictly define
 16 them.

17 - One solution that could be explored would be obtaining a total \mathbf{K}_e decoupling for the 6 states.

18 This additional constraint gives a unique solution.

19 - Another option is to compute the feedback matrix which minimizes a quadratic index
 20 performance based on a combination of states and control values.

- 1 Both possibilities are evaluated in the next sections regarding
- 2 - The performances in rated conditions,
- 3 - The robustness towards parameter uncertainties,
- 4 - The ease of implementation.



5
6 **Fig. 2. Extended system with full state feedback.**

7 4. DECOUPLING STRATEGY

8 This section focuses on the first identified option which consists in dynamically decoupling
 9 [17, 18] the link between current references and current responses. Its specific tuning is explained
 10 and then computed.

11 4.1. Specific tuning leading to a decoupled feedback.

12 Combining the extended state equation (12) and the full feedback control law (13) derives the
 13 close loop behavior described by:

$$\frac{d}{dt} \begin{bmatrix} I \\ Int_{\epsilon} \end{bmatrix} = A_{e,CL} \begin{bmatrix} I \\ Int_{\epsilon} \end{bmatrix} + B_{e,CL} [I_{ref}] \quad (14)$$

14 Where $A_{e,CL}$ represents the $n_e \times n_e$ closed loop state matrix and $B_{e,CL}$ is the $n_e \times n$ closed loop
 15 control matrix. The latter are defined as follows:

$$A_{e,CL} = \begin{bmatrix} A - B \cdot K_{e1} & -B \cdot K_{e2} \\ -Id_3 & \mathbf{0}_3 \end{bmatrix}$$

$$B_{e,CL} = \begin{bmatrix} \mathbf{0}_3 \\ Id_3 \end{bmatrix}$$

The characteristics of the system response is fully determined by the value of the $n \times n_e = 18$ adjustable terms of the closed-loop state matrix, namely the first n rows of this matrix. It is sought to impose:

- First the $n_e = 6$ eigenvalues in order to settle the overall closed loop dynamics. Writing the characteristic equation and identifying it with its desire form leads to $n_e = 6$ non-linear equations.

- Second a cancellation of the coupling effect between the three windings currents. For instance, i_2 and i_3 , as well as $int_{\varepsilon 2}$ and $int_{\varepsilon 3}$, must no longer impact the time-derivative of the first current di_1/dt . In sum, the closed loop matrix must also conform to the following form:

$$A_{e,CL} = \begin{bmatrix} a_{11} & 0 & 0 & a_{14} & 0 & 0 \\ 0 & a_{22} & 0 & 0 & a_{25} & 0 \\ 0 & 0 & a_{33} & 0 & 0 & a_{36} \\ -1 & 0 & 0 & 0 & 0 & 0 \\ 0 & -1 & 0 & 0 & 0 & 0 \\ 0 & 0 & -1 & 0 & 0 & 0 \end{bmatrix} \quad (15)$$

Finally, $(n \times n_e) - n_e = 12$ independent linear equations can be deduced from this imposed matrix structure.

In conclusion, this first strategy leads to solve a system of $n \times n_e = 18$ equations with $n \times n_e = 18$ unknowns.

4.2. Matrix gain related to decoupling strategy.

It can be achieved using a specific solver based on formal calculation or numeric computation.

The latter technique that was used here. The final results are shown in Table 3. Most of the

1 coefficients of the feedback gain matrix K_e are nonzero. None of the square sub-matrices (namely
 2 K_{e1} and K_{e2}) are diagonal which reveals a very coupled feedback. All state variables are really
 3 necessary to compute one of the 3 control values d_k .

4 This finding impacts significantly both the controller implementation and the global system
 5 behavior. Indeed, during large fluctuation of the set point, the control law will temporarily compute
 6 large control values. In practice, the duty cycle will be saturated to its own limits. Saturation causes
 7 an open-loop behavior, which is especially detrimental to integral terms that continue to evolve.
 8 Integral terms then lead to large unexpected overshoot and possibly instability while saturation
 9 occurs. Anti-windup systems [19 - 21] intend to maintain the system in close loop. However,
 10 saturation is a non-linear phenomenon. In the present case of non-diagonal submatrices, it is not
 11 possible to know with certainty which of the integral terms induce saturation. Hence in any
 12 saturation situation the anti-windup system clamps the three integral actions. This conservative
 13 option leads to a sub-optimal implementation of the controller.

14 In sum, the strict decoupling option has two theoretical drawbacks. It leads to a large number of
 15 multiplications and it results in an inadequate anti-windup implementation.

16 Next section presents the second approach, in order to be able to compare them using simulation
 17 MATLAB tool.

18

| K_{e1} | | | K_{e2} | | |
|----------|--------|--------|----------|--------|--------|
| 2.033 | -1.933 | -0.967 | -12 000 | 11 600 | 5 800 |
| -0.967 | 1.067 | -0.967 | 5 800 | -6 400 | 5 800 |
| 0.000 | 0.000 | 3.000 | 0 | 0 | -1 800 |

19
 20 **Table 3. 18 coefficients of the decoupling full state feedback.**

21

1 5. LINEAR QUADRATIC REGULATOR (LQR)

2 5.1. Objective function

3 An alternate way to address the setting parameters design issue of the full state feedback is to
4 settle the degrees of freedom and flexibility using a global performance index summarizing the
5 closed loop behavior. It involves a functional, namely a time infinite-horizon Riemann integral
6 based on a quadratic cost function:

$$J = \int_0^{\infty} \left(\begin{bmatrix} I \\ Int_{\varepsilon} \end{bmatrix}^t \cdot Q \cdot \begin{bmatrix} I \\ Int_{\varepsilon} \end{bmatrix} + D^t \cdot R \cdot D \right) \cdot dt \quad (18)$$

7 Where Q and R are two positive semi-definite matrices of weighting factors for the various state
8 and control components, respectively. As in this case, any current i_k plays the same role and
9 similarly any duty cycle d_k applies the same way, Q and R are simplified to $Q = \begin{bmatrix} Id_3 & 0_3 \\ 0_3 & q \cdot Id_3 \end{bmatrix}$
10 and $R = \rho \cdot Id_3$.

11 In conclusion, the objective is to find the (q, ρ) set of two scalar values that best meets
12 specification (given in Table 2). For this purpose, each (q, ρ) set permits to compute a full state
13 feedback $D = -K_e \cdot [I \quad Int_{\varepsilon}]^t$ that minimizes the cost function:

$$J(q, \rho) = \int_0^{\infty} \left(\begin{bmatrix} I \\ Int_{\varepsilon} \end{bmatrix}^t \cdot \begin{bmatrix} Id_3 & 0_3 \\ 0_3 & q \cdot Id_3 \end{bmatrix} \cdot \begin{bmatrix} I \\ Int_{\varepsilon} \end{bmatrix} + D^t \cdot \rho \cdot Id_3 \cdot D \right) \cdot dt \quad (19)$$

14 To determine the first optimization level, namely the full state feedback settings, Riccati equation
15 is used. The choice of the 2 weighting coefficients is the second step which is realized using a
16 genetic algorithm [11]. It permits to settle the actual degree of freedom of LQR approach.

17 5.2. Matrix gain related to LQR strategy.

18 Based on this LQR design approach [11, 22], the global full state feedback is designed. It leads

1 to the parameters listed in Table 5. It actually seems that most the K_{e2} gain matrix related to the
 2 integral terms is strictly diagonal and that the K_{e1} gain matrix related to the proportional terms has
 3 dominant values in the diagonal line. In concrete terms this means the controller acts as if it was
 4 three independent controllers acting independently on their dedicated duty cycle. In this context, it
 5 leads to a fewer number of multiplication, but above all to a simple and efficient anti-windup
 6 scheme because the reason for a saturation effect can be easily attributed to the related integral
 7 term.

| K_{e1} | | | K_{e2} | | |
|----------|--------|--------|----------|-------|-------|
| 0.564 | -0.154 | -0.154 | -3162 | 0 | 0 |
| -0.154 | 0.564 | -0.154 | 0 | -3162 | 0 |
| -0.154 | -0.154 | 0.564 | 0 | 0 | -3162 |

8
 9
 10 **Table 5. LQR design of the full state feedback strategy setting parameters.**

11 6. COMPARATIVE SIMULATIONS RESULTS

12 To illustrate the dynamic properties of both feedback design approaches, this section shows the
 13 closed loop system response while it is subject to three specific current reference changes, namely
 14 stimulation of the common mode, of the differential modes and finally of both modes. The initial
 15 condition is set so that the converter provides 6 A to the load (200 V voltage source) equitably
 16 shared by the three ICT windings (2 A). This equilibrium point corresponds to 3 duty cycles close
 17 to 50%.

18 In this first step, the system is considered with the same rated parameters as those used to tune
 19 the controller.

20 6.1. Common mode response.

21 For this trial, all current references have a similar 500 Hz square generator with 2 A as low level
 22 and 4 A as high level. Figure 3 reports the corresponding results of both strategies.

1 As planned by the decoupling theory, the winding currents evolve simultaneously while
2 satisfying the $500 \mu s$ time settling requirement, as shown in Figure 3 a). The common-mode and
3 differential-mode currents confirm this assessment by showing no response on the two differential
4 mode channels. To get this effect, the controller only slightly changes the duty cycle amplitude
5 which is consistent with the small common mode open-loop time constant.

6 Figure 3 b) shows the LQR results. It also complies with the $500 \mu s$ time settling requirement,
7 having faster time response than the previous one. As an illustration of this phenomenon, it can be
8 noticed that the control overshoot values are roughly 60% higher than in the decoupling case.
9 Nevertheless, as in this last case, the control value fluctuations remain low.

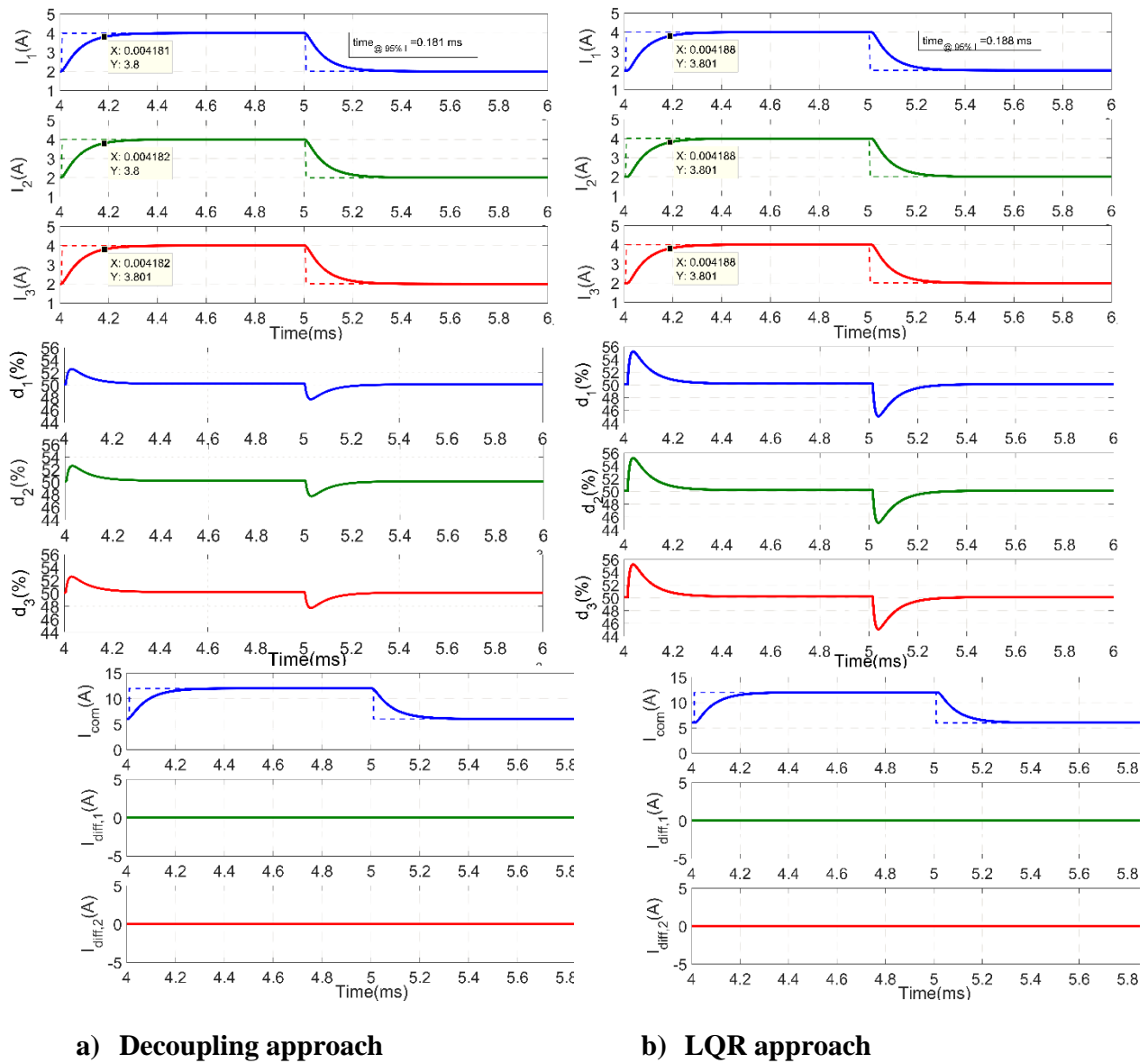


Fig. 3. Closed loop common mode response.

1

2 6.2. Differential mode response.

3 Figure 4 shows the results of the situation where the first current reference $i_{1,ref}$ has a $2/3 A$

4 ripple magnitude while the two others are set in opposite phase with half the magnitude, namely

5 $1/3 A$.

1 Regarding the decoupling approach depicted in Figure 4 a), each current has the same dynamics
2 as the common mode one. On the other hand, the different duty cycles have a large transient
3 overshoot which is explained by the need to compensate the slow natural differential mode
4 dynamics. Indeed the natural response time value is thirty times higher than the common mode
5 one. Anyway, as expected by the theoretical part, the fictitious currents show a unique mode
6 evolution (first differential mode) while the two other channels (i.e. common mode and second
7 differential mode) have no reaction. The closed loop decoupling is therefore entirely satisfied.

8 The LQR approach shows different results. As demanded by the specification, the differential
9 mode satisfies the 500 μ s time settling requirement, but it has a slower dynamics than the common
10 mode one. Contrary to the previous strategy, the LQR method derives a control that makes both
11 modes dynamics different. This result is not surprising given that LQR has a global approach
12 combining both error and control magnitudes issues. As differential mode is slow, it provides the
13 minimum required gain values. As already noted, these gain values make the common mode faster
14 due to its intrinsic high dynamics. It can be noticed in figure 4 that the control overshoot values are
15 roughly 15% lower than in the decoupling case. This tuning difference would have an impact on
16 the single step response illustrating the case of a desired channel mismatch due to cell
17 discrepancies, such as cell overheating. This further trial activates simultaneously both common
18 and differential modes.

19

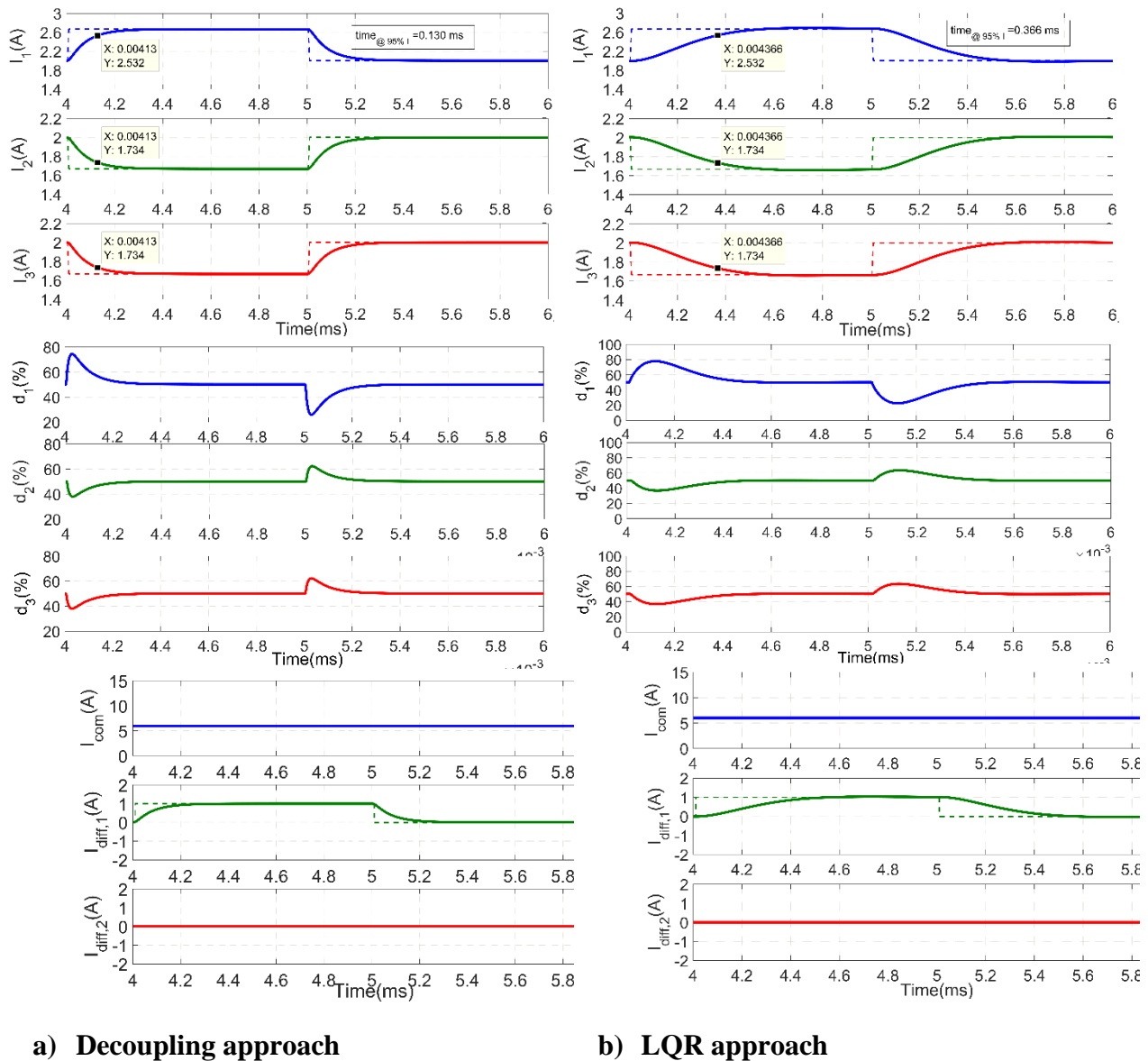


Fig. 4. Closed loop differential mode response.

1
 2 6.3. Single mode response.
 3 Finally, figure 5 and figure 6 depict the results corresponding to the configuration where the
 4 supervision strategy needs to use unbalanced windings currents, for instance to take the pressure
 5 off a warmer cell. To make this last point, only the first current reference $i_{1,ref}$ changes with a step

1 magnitude of $2A$ (see figure 5) and then $3A$ (see figure 6). This trial solicits both the common mode
2 and the first differential mode.

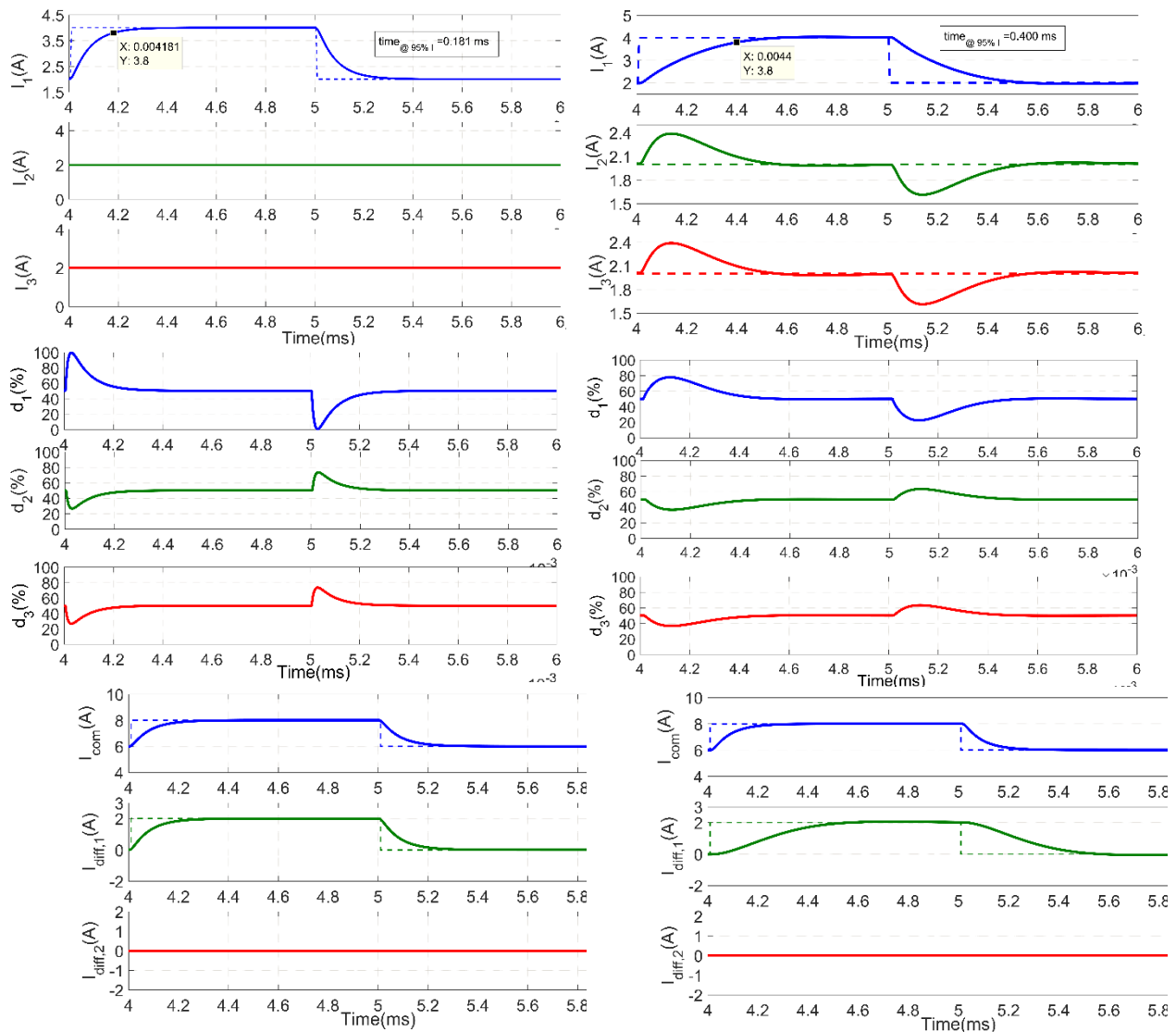
3 As far as the decoupling strategy is concerned, the first trial shows input-output decoupling
4 resulting from the fact that each natural mode behaves with similar time response. As this situation
5 solicits two out of the three system modes, it is also not surprising to note that duty cycles react
6 strongly. However figure 6 shows a coupling effect. That has been tied to the fact that one duty
7 cycle tends transiently to exceed its limit value: the anti-windup apparatus operates and introduces
8 a non-linearity which cancels the decoupling effect. This phenomenon disappears as soon as anti-
9 windup function is useless.

10 Figure 5 b) depicts the first current step response behavior of the LQR method. Compared to
11 figure 5 a), the LQR design induces a much less aggressive control law which maintains the duty
12 cycles much easily within its limits. Conversely, the first current change impacts slightly the two
13 others without exceeding the specifications. It arises because the common mode and differential
14 mode dynamics are different this time.

15 Figure 6 b) also illustrates that the present controller may be almost considered as composed of
16 three independent controllers. Indeed, figure 6 b) shows in dashed lines the same transient response
17 in the case where all non-diagonal terms of K_{e1} are set to zero. Even if the coupling effects is
18 somewhat increased, the behavior remains similar and totally acceptable. That is the reason why
19 the anti-windup apparatus can be properly built by impacting solely the integral term corresponding
20 to the control variable in saturation. Moreover it leads to a very simple implementation similar to
21 SISO systems. Figure 6-b depicts the very good functioning of this implementation. It should be
22 specified that the step magnitude has to be enlarged in figure 6 b) compared to figure 6 a), in order
23 to reach saturation mode. It is clearly due to the less aggressive behavior of the LQR approach

1 compared to the decoupling one. For information, in the present case, only the first duty cycle is is
 2 saturated and consequently the first integer is stopped simply if the first duty cycle is clamped to
 3 100% and the current error is positive, or the first duty cycle is clamped to 0% and the current error
 4 is negative.

5



a) Decoupling approach

b) LQR approach

Fig. 5. Closed loop single step response : small signal

1
2

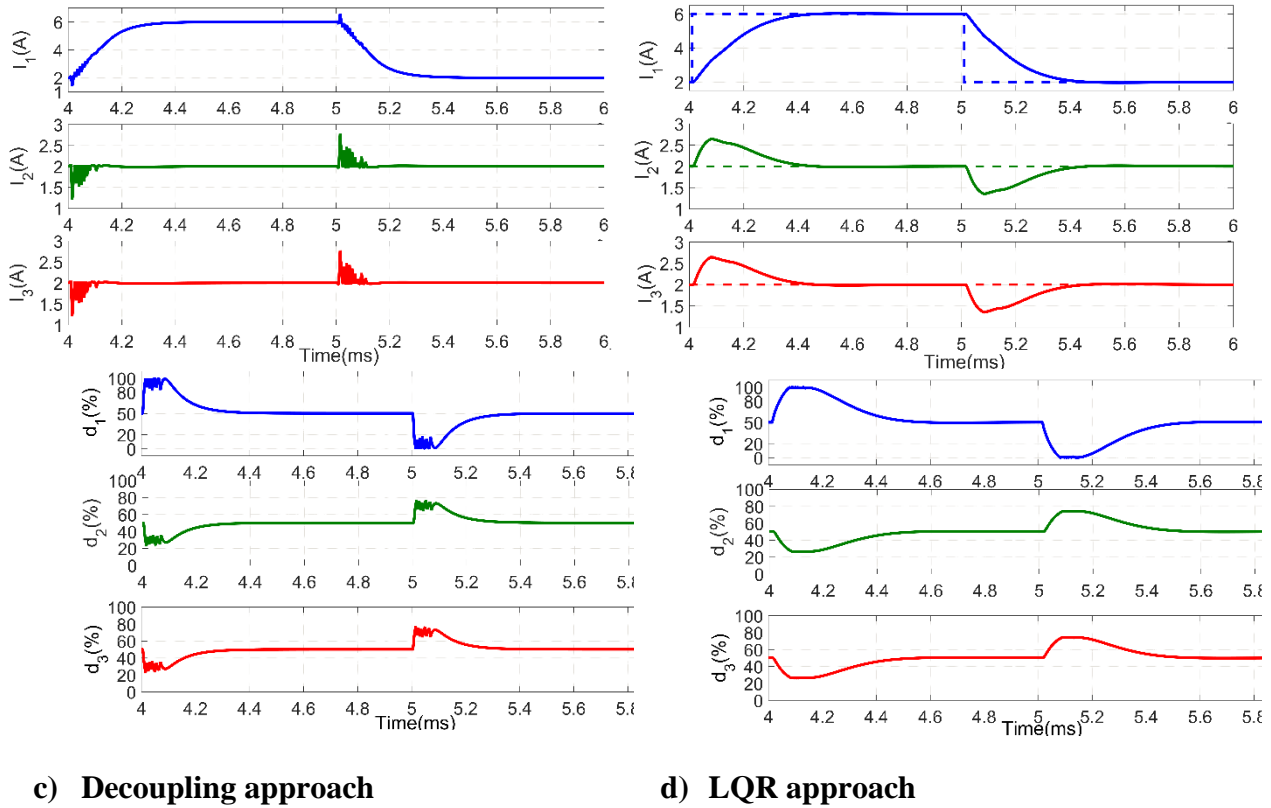


Fig. 6. Closed loop single step response : large signal

3

4 6.4. Sensitivity analysis.

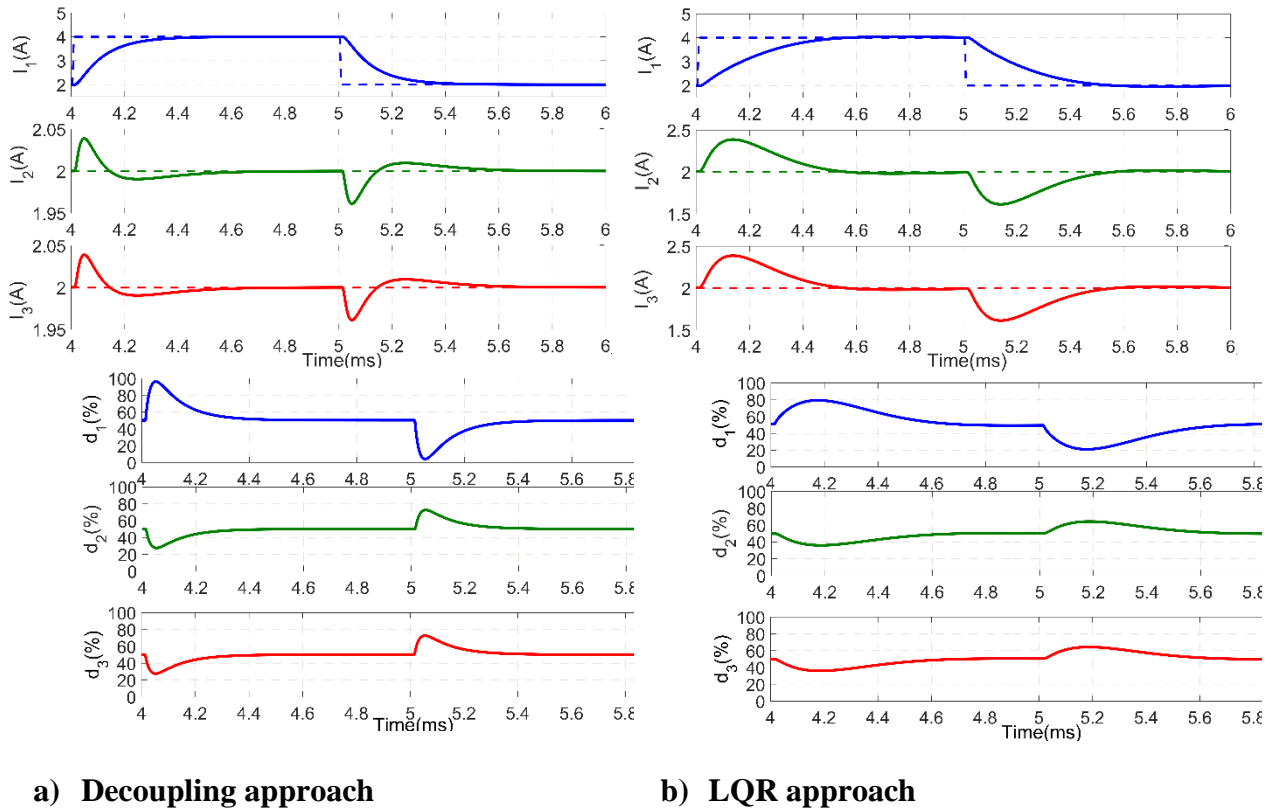
5 This second step investigates the sensitivity of both designs towards ICT parameters. Self-
 6 inductance and mutual inductance are studied as critical parameters to assess the control robustness.

7 Considering decoupling design, a better ICT coupling cancels the perfect coupling rejection as
 8 depicted in figure 7-a where the actual values are $l = 19.8\text{mH}$ and $m = 9.7\text{mH}$. It induces a shift
 9 of the natural common mode dynamics (smaller time response) which finally also induces a close
 10 loop common mode settling time. This change is mitigated by the controller but it induces a

1 mismatch between the different modes dynamics which in turn produces this temporal channel
 2 coupling effect. In the case of an even better ICT coupling, the close loop behavior can also face
 3 instability as reported in figure 8-a, where $l = 19.7\text{mH}$ and $m = 9.8\text{mH}$.

4 Besides a smoother control action and a simpler implementation in a controller, the LQR design
 5 proves a better robustness regarding parameters uncertainty. As a matter of fact, figure 7-b and
 6 figure 8-b show that the controller remains stable even in the most demanding case of a higher
 7 actual ICT coupling than expected, namely when $l=19.7\text{mH}$ and $m=9.8\text{mH}$.

8



a) Decoupling approach

b) LQR approach

**Fig. 7. Closed loop single step response with small ICT parameters change.
 ($L = 19,8 \text{ mH}$ and $M = 9,7 \text{ mH}$)**

9

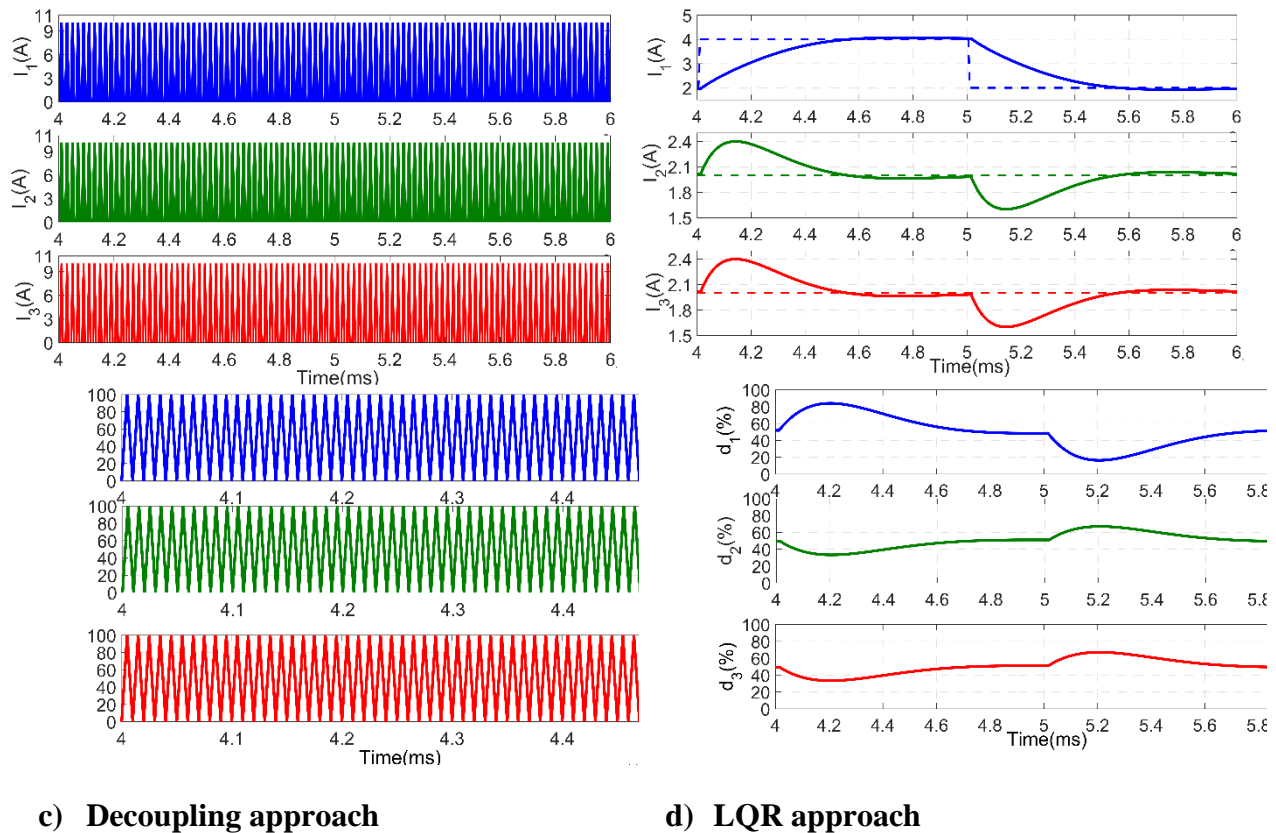


**Fig. 8. Closed loop single step response with small ICT parameters change.
 (L = 19,7 mH and M = 9,8 mH)**

1
 2 6.5. Overview of the simulation results.
 3 In summary, it can be said that the decoupling strategy leads to a controller easy to implement
 4 with a modal approach. However, it reveals limited in the case of a good ICT coupling because it
 5 requires high gains to boost low natural dynamics, namely differential mode, and becomes hence
 6 sensitive to noise injection and sampling effects. In addition, the real implementation does not
 7 exhibit a very efficient anti-windup scheme. Last but not least, the closed loop behavior is
 8 somewhat sensitive to parameters which is not appropriate for a robust control. That is why linear
 9 quadratic regulator [11, 24] design is much better to considered. It respects the various
 10 specifications demand, provides smooth control in the present case of a large range of natural

1 dynamics and ensures a very robust response towards parameters change.

2 **7. CONCLUSION AND PERSPECTIVES**

3 The present study addresses the easier and more robust way to implement a controller scheme
4 dedicated to control the current in an interleaved multi-cell converter using an ICT. The study is
5 based on a specific 3-cell converter, but it draws generalizable conclusions about control of
6 interleaved converters, whatever the number of cells. ICT device clearly enables to significantly
7 reduce both input and output currents ripples which permits using reliable capacitor technology.
8 However, the ICT magnetic coupling induces to deal with a real MIMO system. To cope with this
9 issue, two different approaches are assessed.

10 The first one based on a modal method is easy to understand for an engineering point of view.
11 While operating in linear mode and with rated values, it permits a very good decoupling between
12 the references inputs and the related outputs. However, an efficient anti-windup scheme cannot be
13 implemented to optimally take the duty cycles saturation into account. Moreover, the control design
14 reveals somewhat sensitive to the ICT parameters which may be difficult to evaluate precisely.
15 Finally, it uses high gains to offset the slow natural dynamics of the differential mode, possibly
16 leading to noise sensitivity and more frequent saturated behavior.

17 The second methodology is based on a full state feedback of an extended model whose
18 parameters are set using a quadratic cost time function. This so-called LQR technique enables to
19 find a good trade-off between the different key points of the specification, which are stability,
20 settling time, decoupling and robustness. Although a small but acceptable coupling remains, this
21 second controller exhibits an almost internally decoupled structure permitting to implement a
22 simple and efficient anti-windup technique. In addition, the controller acts smoothly during
23 transient which reduces noise sensitivity. Finally it reveals more robust to ICT parameters changes,

1 which is an important asset.

2 All these studies carried out in simulation show that the interleaved multi-cell converter is a very
3 specific power converter. In this particular case, the full state feedback approach based on LQR
4 method exhibits a very attractive trade-off between the different requirements of the control
5 specifications while enabling a very easy implementation in a microcontroller or a FPGA device.
6 These very positive results encourage to validate the study with an experiment on a laboratory test
7 bench.

8 From a broader perspective, the present work shows to the power electronics community that
9 there is a genuine benefit in switching from decoupling approach to LQR methodology. Whatever
10 the system under study, decoupling strategy is proving to be much more sensitive to parameter
11 changes and provides larger control values in case of a significant difference between natural
12 dynamics. Conversely, if some small cross-coupling may be permitted, LQR tuning provides a
13 robust and smooth control, which is extremely satisfying from an engineering point of view.

14 **REFERENCES**

- 15 [1] E. Laboure, A. Cuniere, T. A. Meynard, F. Forest and E. Sarraute, "A Theoretical Approach
16 to InterCell Transformers, Application to Interleaved Converters", IEEE Transactions on
17 Power Electronics, vol. 23, no. 1, pp. 464-474, Jan. 2008.
- 18 [2] Y. Cho, "Dual-buck residential photovoltaic inverter with a high-accuracy repetitive current
19 controller", Renewable Energy, vol. 101, pp. 168-181, Feb. 2017.
- 20 [3] D. Guilbert, A. Gaillard, A. N'Diaye, and A. Djerdir, "Power switch failures tolerance and
21 remedial strategies of a 4-leg floating interleaved DC/DC boost converter for
22 photovoltaic/fuel cell applications", Renewable Energy, vol. 90, pp. 14-27, May 2016.

- 1 [4] N. Zhang, D. Sutanto, and K. M. Muttaqi, “A review of topologies of three-port DC–DC
2 converters for the integration of renewable energy and energy storage system”, *Renewable
3 and Sustainable Energy Reviews*, vol. 56, pp. 388-401, Apr. 2016.
- 4 [5] D. Guilbert, A. N'Diaye, A. Gaillard, and A. Djerdir, “Fuel cell systems reliability and
5 availability enhancement by developing a fast and efficient power switch open-circuit fault
6 detection algorithm in interleaved DC/DC boost converter topologies”, *International
7 Journal of Hydrogen Energy*, vol. 41, pp. 15505-15517, Sept. 2016.
- 8 [6] M. Elsied, A. Oukaour, H. Chaoui, H. Gualous, R. Hassan, and A. Amin, “Real-time
9 implementation of four-phase interleaved DC–DC boost converter for electric vehicle
10 power system”, *Electric Power Systems Research*, vol. 141, pp. 210-220, Dec. 2016.
- 11 [7] S. Sanchez, F. Richardeau, and D. Risaletto, “Design and fault-operation analysis of a
12 modular cyclic cascade inter-cell transformer (ICT) for parallel multicell converters”,
13 *Mathematics and Computers in Simulation*, vol. 131, pp. 190-199, Jan. 2017.
- 14 [8] M. L. Bolloch, M. Cousineau, and T. Meynard, “Current-sharing control technique for
15 interleaving VRMs using intercell transformers”, in *2009 13th European Conference on
16 Power Electronics and Applications*, 2009, pp. 1-10.
- 17 [9] C. Gautier, F. Adam, E. Laboure, B. Revol, and D. Labrousse, “Control for the currents
18 balancing of a multicell interleaved converter with ICT”, in *2013 15th European
19 Conference on Power Electronics and Applications (EPE)*, 2013, pp. 1-9.
- 20 [10] B. Amghar, M. Darcherif, J.-P. Barbot, and P. Gauthier, “Modeling and control of parallel
21 multicell chopper using Petri nets”, *IFAC Proceedings Volumes*, vol. 45, pp. 633-638, Nov.
22 2012

- 1 [11] F. H. Dupont, V. F. Montagner, J. R. Pinheiro, H. Pinheiro, S. V. G. Oliveira and A. Péres,
2 “Comparison of Linear Quadratic Controllers with Stability Analysis for DC-DC Boost
3 Converters Under Large Load Range”, Asian J. Control, Vol. 15, No. 3, pp. 861–871, May
4 2013.
- 5 [12] Yu Li and Masato Ishikawa, “Statistical Analysis of Power System Sensitivity Under
6 Random Penetration of Photovoltaic Generation”, Asian J. Control, Vol. 19, No. 5, pp. 1–
7 11, Sept. 2017.
- 8 [13] M. Shahin and S. Maka, “State variable approach to the analysis of neural control of long
9 term blood pressure dynamics”, Asian Journal of Control, Vol. 13, No. 1, pp. 164 176, Jan.
10 2011
- 11 [14] N. Yassa, M. Rachek, “Modeling and detecting the stator winding inter turn fault of
12 permanent magnet synchronous motors using stator current signature analysis”,
13 Mathematics and Computers in Simulation, 2018,in press
- 14 [15] E. Ostertag, “Mono- And Multivariable Control and Estimation”, Springer, 5 January 2011,
15 ISBN-10: 3642137334.
- 16 [16] W. M. Wonham, “On pole assignment in multi-input controllable linear systems”, IEEE
17 Trans. Autom. Control, Vol. 12, pp. 660–665, Dec. 1967.
- 18 [17] T.G. Pimenides, S.G. Tzafestas, “Feedback decoupling-controller design of 3-D systems in
19 state space”, Mathematics and Computers in Simulation, Vol. 24, N° 4, 1982, pp 341-352.
- 20 [18] J. Ruiz-Leon, A.J. Sapiens, S. Čelikovsky and J.A. Torres, “Decoupling with stability:
21 application to the real time control of a water storing plant”, Asian J. Control, Vol. 6, No. 3,
22 pp. 415-420, Sept. 2004.

- 1 **[19]** Frederik M. De Belie, Peter Sergeant, Jan A. Melkebeek, “A sensorless PMSM drive using
2 modified high-frequency test pulse sequences for the purpose of a discrete-time current
3 controller with fixed sampling frequency”, *Mathematics and Computers in Simulation*,
4 Vol. 81, N° 2, 2010, pp 367-381.
- 5 **[20]** C. L. Hoo, Sallehuddin Mohamed Haris, Edwin C. Y. Chung and Nik Abdullah Nik
6 Mohamed, “New Integral Antiwindup Scheme for PI Motor Speed Control”, *Asian J.*
7 *Control*, Vol. 17, No. 6, pp. 2115–2132, Nov. 2015.
- 8 **[21]** K. Suyama and N. Sebe, “Controller Reset Strategy for Anti-Windup Based on Switching
9 L2 Gain Analysis”, *Asian J. Control*, Vol. 20, No. 1, pp. 1–14, March 2018
- 10 **[22]** Wah Soon Lee, Machavaram Venkata Calapathy Rao, “Modeling and design of tape
11 transport mechanism”, *Mathematics and Computers in Simulation*, Vol. 72, N°1, 2006,
12 pp. 26-37.